pollutants

MDPI

Article

Assessing a Large-Scale Sequential In Situ Chloroethene Bioremediation System Using Compound-Specific Isotope Analysis (CSIA) and Geochemical Modeling

Giulia Casiraghi, Daniele Pedretti *, Giovanni Pietro Beretta, Marco Masetti and Simone Varisco

Dipartimento di Scienze della Terra "A. Desio", Università degli Studi di Milano, 20133 Milano, Italy
* Correspondence: daniele.pedretti@unimi.it

Abstract: Compound-specific isotopic analysis (CSIA) and geochemical modeling were applied to evaluate the effectiveness of an 800 m-long sequential in situ bioremediation (ISB) system in Northern Italy. The system was created for the clean-up of a polluted aquifer affected by chloroethenes. A hydraulically upgradient anaerobic (AN)-biobarrier-stimulated reductive dichlorination (RD) of higher chloroethenes (PCE, TCE) and a downgradient aerobic (AE)-biobarrier-stimulated oxidation (OX) of lower chloroethenes (DCE, VC) were proposed. Carbon CSIA and concentration data were collected for PCE, TCE, cis-DCE and VC and interpreted using a reactive transport model that was able to simulate isotopic fractionation. The analysis suggested that the combination of CSIA and modeling was critical to evaluate the efficiency of sequential ISBs for the remediation of chloroethenes. It was found that the sequential ISB could reduce the PCE, TCE and cis-DCE concentrations by >99% and VC concentrations by >84% along the flow path. First-order RD degradation rate constants (k_{RD}) increased by 30 times (from k_{RD} = 0.2–0.3 y^{-1} up to k_{RD} = 6.5 y^{-1}) downgradient of the AN barrier. For cis-DCE and VC, the AE barrier had a fundamental role to enhance OX. First-order OX degradation rate constants (k_{OX}) ranged between k_{OX} = 0.7–155 y^{-1} for cis-DCE and k_{OX} = 1.7–12.6 y^{-1} for VC.

Keywords: chloroethenes; enhanced bioremediation; anaerobic organohalide respiration; aerobic oxidative biodegradation; landfill; compound-specific stable isotope analysis; reactive transport model; PHREEQC

Citation: Casiraghi, G.; Pedretti, D.; Beretta, G.P.; Masetti, M.; Varisco, S. Assessing a Large-Scale Sequential In Situ Chloroethene Bioremediation System Using Compound-Specific Isotope Analysis (CSIA) and Geochemical Modeling. *Pollutants* **2022**, *2*, 462–485. https://doi.org/10.3390/pollutants2040031

Academic Editors: Hongbiao Cui, Yu Shi, Haiying Lu, Lin Chen and Ru Wang

Received: 26 August 2022
Accepted: 21 October 2022
Published: 11 November 2022

1. Introduction

In situ bioremediation (ISB) is an effective solution for the treatment of polluted waters directly in the aquifer [1–4]. ISB relies on the control of microbially mediated reactions that affect the stability of organic pollutants, such as chloroethenes, in soils. Metabolic and co-metabolic processes concur to transform organic waste into harmless compounds, such as biomass, CO_2 or CH_4 [5].

A potential limitation of ISB is that typical systems are tuned to stimulate one specific type of biodegradation, i.e., either reductive dechlorination (RD) or oxidative degradation (OX) [3]. However, whilst higher chlorinated ethenes (tetrachloroethene (PCE) and trichloroethene (TCE)) are better degraded through RD, lower chlorinated ethenes (dichloroethene (DCE) and vinyl chloride (VC)) are instead recalcitrant to RD and more easily degraded through OX. As DCE and VC are "daughter" products of the RD of the "parent" species PCE and TCE, they tend to accumulate in aquifers if only RD is stimulated. The accumulation of VC is particularly problematic since it is a known human cancerogenic compound with greater toxicity than the other chloroethenes [6].

"Sequential" ISB [3,7–9] was proposed to attain complete degradation of all chloroethenes, circumventing the limitation of a "single" ISB system. The design of a sequential ISB system involves two "biobarriers". A hydraulically upgradient biobarrier is designed to attain anaerobic conditions, favoring RD. The byproducts of RD are transported toward a

downgradient biobarrier, which stimulates OX. This combined approach aims at achieving complete dechlorination of all chloroethenes, reducing the likelihood of accumulating undesired intermediate products, particularly VC.

Despite having been idealized several years ago, only a few documented operational-scale sequential ISBs have been presented so far [3]. From a hydrogeological perspective, this may be partly linked to two reasons.

1. *Lack of model-based analyses of sequential ISBs.* Mathematical models are particularly important to provide quantitative support for decision makers [4,10–14]. As the usefulness of mathematical tools was already demonstrated for single ISBs [14–17], we maintain that such models could also be fundamental for the correct design and implementation of sequential ISBs. While coupled biogeochemical and hydrogeological modeling was traditionally computationally prohibitive, we highlight that modern workstations have considerably alleviated the computational burden and multiple open-source codes are now available [18] to efficiently reproduce the main processes involved in an ISB. Moreover, in most bioremediation studies, one-dimensional (1-D) reactive transport models (RTMs) are utilized, i.e., solute transport models that couple 1-D flow dynamics and geochemical processes [18]. Such models are useful to identify geochemical processes that occur along individual flow paths [19], limiting the computational demand compared with more challenging multidimensional models.
2. *Lack of studies applying compound-specific isotope analysis (CSIA) to sequential ISBs.* In the presence of organic compounds that undergo parent–daughter reaction chains, transformation reactions produce an enrichment of heavy isotopes in the parent compound and the formation of isotopically lighter products [20]. The combined use of compound-specific carbon isotope analysis (C-CSIA) and concentration data can provide a more complete and precise evaluation of the biodegradation processes occurring at a site than the analysis of concentration data alone [15,21]. Therefore, the use of CSIA could be highly valuable for the evaluation of sequential ISBs. For instance, it could help to detect the occurrence of anaerobic or aerobic degradation; evaluate potentially interfering mechanisms, such as the mixing of waters undergoing different degradation pathways; or provide constraints for the development of mathematical models [15].

This work presents and analyses the results of multiyear monitoring of an 800 m-long sequential ISB system in Italy. This ISB system was created for the cleanup of an alluvial aquifer that was severely contaminated by a plume of PCE and byproducts that originated from an old industrial landfill. After several years of small-scale experimental activities on and off site [22], a full-scale sequential ISB was installed. It is currently Italy's largest sequential ISB, and arguably the largest-scale facility of the world of this kind. The goal of this work was to improve the current state-of-the-art regarding the use of advanced characterization and modeling tools, mainly through the evaluation of concentration time series, CSIA data and RTM to gain insight into the effectiveness of the sequential ISB system, identifying processes and quantifying reaction rates occurring at the site.

2. Materials and Methods

2.1. Background Information

The polluted aquifer object of this study is located in Northern Italy, in the proximity of a lagoon (Figure 1a). The ground level is below the sea level (between −0.3 m and −1 m a.s.l.). The site is bounded by the lagoon to the south and by an agricultural land reclamation canal (ALRC) to the north. The ALRC is an artificial drainage system that permits the reclamation of the land between the lagoon and the ALRC itself.

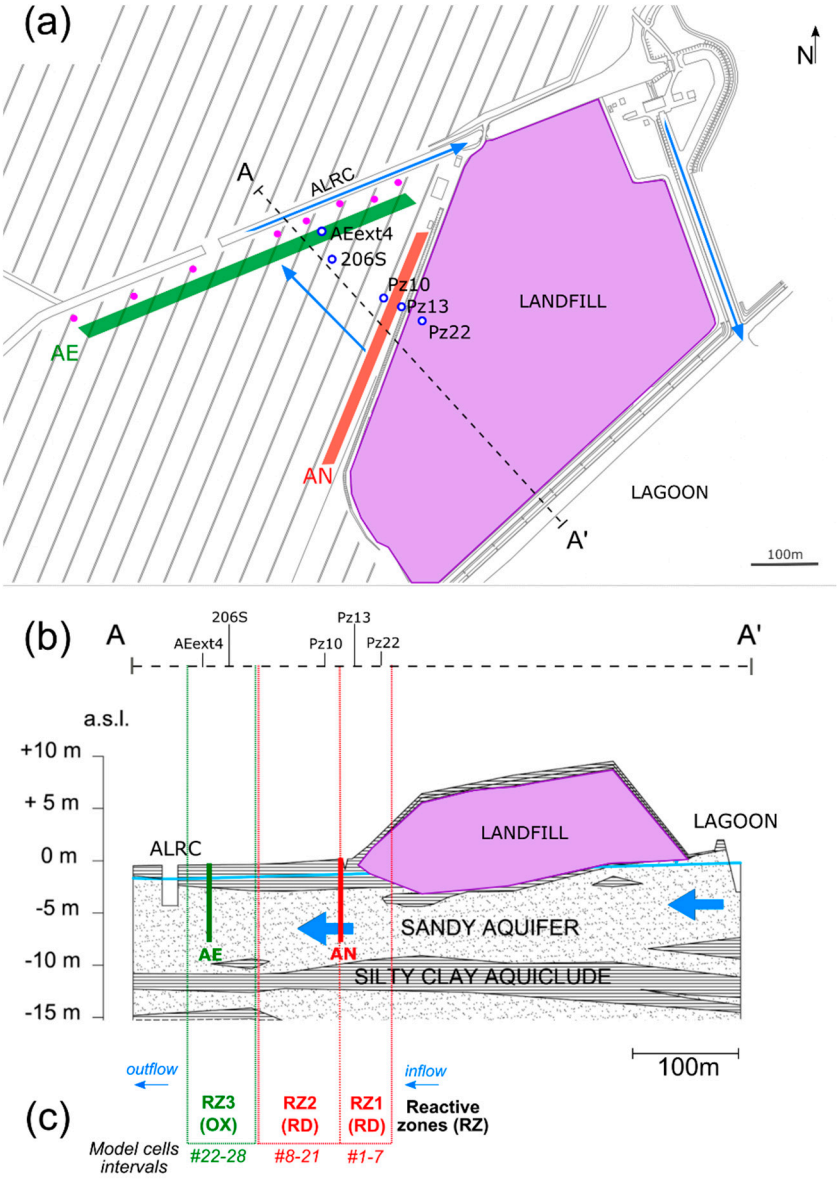

Figure 1. (**a**) Map of the study area, showing the landfill (lilac area) and the position of the ISB systems (AN—anaerobic barrier, AE—aerobic barrier) and the five boreholes utilized in the analysis. The wells of the P&T system are represented as purple dots. (**b**) Schematic geological cross-section of the study area (corresponding to the A–A' trace indicated in (**a**)), highlighting the top aquifer (first 10–12 m from the ground surface). The vertical axis represents the topographic elevation above sea level (a.s.l.). The blue arrows indicate the groundwater flow direction, which was oriented from the lagoon in the southeast to the agricultural land reclamation canal (ALRC) in the northwest. (**c**) Conceptual scheme of the PHREEQC model, highlighting the three reactive zones defined by the corresponding cell intervals. In RZ1 and RZ2, reactions were mainly controlled by reductive dechlorination (RD), while in RZ3, oxidation (OX) prevailed.

Geologically, the subsurface is characterized by stratified alluvial deposits composed of alternated sandy and silty clay layers (Figure 1b). From the ground surface down to about 9–12 m depth, silty fine sand and sandy silt with rare medium sand lenses form the shallow aquifer, which is capped by a surficial layer of silty clays and clayey silts up to 3 m thick. The low permeability layer is locally absent, making the aquifer unconfined or semi-confined based on the spatial continuity of such layer. The geological configuration is similar to that of other adjacent sites described by [23–25].

The contaminated part of the aquifer is limited to the top 12 m from the ground surface. Here, groundwater flows from the lagoon to the ALRC, crossing a former industrial landfill that is responsible for contamination via aromatic hydrocarbons and chloroethenes. Although the landfill was closed in the 1970s, the solute plume was detected for the first time only in 2001. To date, the landfill keeps releasing contaminants into the groundwaters, which exceed the maximum contaminant levels (MCL) established by the Italian law for PCE and its degradation products.

The first characterization and monitoring that led to the installation of the ISB started in 2014 when microbiological laboratory analyses and in situ biodegradation tests were carried out. These investigations are described in detail by Casiraghi et al. [22] and unpublished reports, from which we extracted the following key information.

1. Initial microbiological molecular surveys detected the presence of organohalide-respiring bacteria *Dehalobacter restrictus* and *Dehalococcoides ethenogenes* on site, demonstrating the potential of the site to sustain RD of chloroethenes. *Dehalobacter restrictus* is known to dechlorinate highly chlorinated compounds, such as PCE and TCE [26]. *Dehalococcoides ethenogenes* can also transform less chlorinated compounds, such as DCE and VC to ethene [26].
2. However, anaerobic and aerobic microcosms suggested that natural biodegradation was insufficient to achieve a reduction in concentrations of PCE and its degradation products below the Italian MCL. The addition of reducing substrates in anaerobic microcosms and nutrients containing N and P in aerobic microcosms showed that stimulated biodegradation was much more effective, leading to concentrations that were generally below the MCL.
3. Pilot-scale in situ biodegradation tests confirmed the laboratory results. On-site tests demonstrated that a sequential anaerobic and aerobic treatment could attain a high degradation efficiency of all chloroethenes under biostimulated conditions in the field. For the most chlorinated compounds, such as PCE and TCE, the concentrations dropped to values close to the MCLs.
4. At the end of the experimental activities, further microbiological analyses detected the presence of "aerobic bacteria" that were able to degrade toluene, chlorobenzene, benzene and VC. These bacteria were found within and outside the aerobic pilot site, suggesting that natural aerobic biodegradation of organic compounds could also occur in other parts of the site. Moreover, the abundance of such bacteria was higher inside the pilot site, demonstrating the efficiency of the aerobic treatment in stimulating aerobic degradation.

Based on the successful results from the experimental analyses, an operational scale ISB was set up in 2016 (Figure 1). The ISB is composed of two biobarriers, each consisting of numerous injection and extraction wells arranged in rows. Each set of wells covers a linear distance of about 400 m. Hydrogeologically, the two barriers are arranged sequentially according to their position related to the source (i.e., the landfill).

The "anaerobic" (AN) barrier (red in Figure 1) consists of 20 injection wells and 19 extraction wells and is located close to the landfill. The wells run parallel to the landfill and serve for the extraction of groundwaters and their reinjection in the aquifer after the addition of molasses as a biostimulating compound. The fermentation of the carbohydrates in the molasses produces hydrogen [27], which acts as an electron donor in anaerobic microbial activities. Dissolved oxygen is the first terminal electron acceptor (TEA) to be consumed, followed by nitrate, manganese (IV), iron (III), sulfate and carbon dioxide. This process of TEA consumption leads to progressively more reducing conditions in the aquifer, promoting the RD of chloroethenes, which is most efficient under sulfate reducing and methanogenic conditions [28]. The rate of water recirculation of the whole barrier is about 3.8 m^3h^{-1} and the rate of substrate injection is 2.9×10^{-3} m^3h^{-1}.

The "aerobic" (AE) barrier (green color in Figure 1) is located hydraulically downgradient of the AN barrier and runs parallel to the ALRC. It consists of 39 pumping wells (19 for water extraction and 20 for water reinjection) and 60 air-sparging wells. The extracted water

is dosed with an organic substrate and then reinjected through the injection wells. The average distance between neighboring wells is approximately 10 m. For each air-sparging well, the average injected air flow rate is 2.04 m^3h^{-1}, for a total of $1.22 \cdot \times 10^3$ m^3h^{-1} along the whole barrier. The rate of water recirculation of the whole barrier is about 2.8 m^3h^{-1}.

The bioremediation system is coupled to a pump-and-treat (P&T) system located downgradient of the AE barrier and parallel to the ARCL. The goal of the P&T is to abate the residual contaminant concentrations that the ISB system did not manage to bring under the MCL.

2.2. Hydrochemical and Isotopic Analyses

Our research focused on the monitoring activities performed bimonthly from May 2016 to January 2022 (for a total of 33 sampling campaigns) on five boreholes (Pz22, Pz13, Pz10, 206S and AEext4 in Figure 1) lying along a hypothesized aquifer flow path (parallel to the blue arrow in Figure 1) crossing both barriers, which was determined through the interpretation of the aquifer hydraulic heads distribution in the site. These specific boreholes were selected due to their positions relative to the barriers (upgradient and downgradient), which were expected (according to the rationale of the ISB system) to affect the concentrations and isotopic compositions of chloroethenes through stimulation of different degradation processes. Specifically:

- Pz22 was close to the landfill and far upgradient of the AN and AE barriers. Hence, chloroethenes concentrations and isotopic compositions at Pz22 should be representative of the source conditions.
- Pz13 was located at a distance d = 30 m from Pz22, immediately upgradient of the AN barrier and far upgradient of the AE barrier. Hence, chloroethenes at Pz13 should be mainly affected by natural degradation.
- Pz10 was located at d = 60 m from Pz22, immediately downgradient of the AN barrier, but upgradient of the AE barrier. Chloroethenes at Pz10 should therefore be affected by anaerobic biostimulation and no aerobic biostimulation was expected here.
- 206S was located at d = 164 m from Pz22, further downgradient of the AN barrier and immediately upgradient of the AE one. Here, the transition from RD to OX of chloroethenes took place.
- AEext4 was located at d = 200 m from Pz22, downgradient of the AE barrier and upgradient of the P&T wells. Chloroethenes at AEext4 should be mainly affected by OX.

At these boreholes, environmental parameters, such as pH, Eh, electric conductivity and temperature, were measured through a multiparametric probe. Chemical parameters were estimated in the laboratory through standardized methods. Nitrate and sulfate (SO_4) were determined with the APAT CNR IRSA 4020 Man 29 2003 method. Nitrate concentrations remained below the detection limits for almost the totality of the sampling campaigns (data not reported). Ammonium (NH_4) was determined with the APAT CNR IRSA 4030 A1 Man 29 2003 method. Iron (Fe) and manganese (Mn) were determined with the EPA 6020B 2014 method. Determination of contaminant concentrations was carried out by a laboratory that specialized in environmental analysis with headspace gas chromatography/mass spectrometry (GC/MS) using EPA reference methods 5021A 2014 and 8260D 2018.

In January and May 2021, carbon-compound-specific isotope analysis (C-CSIA) was carried out to determine the isotopic composition (expressed as $\delta^{13}C$) of PCE, TCE, cis-DCE and VC. In January, the analyses were conducted on groundwater samples collected at Pz22, Pz13, 206S and AEext4. In May, the analyses were repeated on the same piezometers and also carried out at Pz10. For each sampling point, three 40 mL vials were filled without a headspace and sealed with Teflon-lined caps. Sodium azide (NaN_3) was added to each vial as a preservative. The analyses were conducted at the Isotope Tracer Technologies Europe (Milan, Italy) laboratory by ITEX/SPME gas chromatograph/isotope ratio mass

spectrometry system (GC/IRMS). Laboratory standards referenced against the international standard Vienna Pee Dee Belemnite were used for the $\delta^{13}C$ determination.

2.3. Geochemical Model

We implemented a one-dimensional (1-D) advective–dispersive–reactive transport model to analyze the degradation of chloroethenes in the field, focusing on the control of the two biobarriers on the different degradation rates and isotope fractionation. To this end, we set up a model that was able to reproduce both the concentrations and $\delta^{13}C$ of the chloroethenes measured in the five selected boreholes. The simulations were conducted using PHREEQC version 3 [29], which is a widely adopted computer code that can reproduce all the required physical and biochemical processes that occur in typical bioremediation systems (e.g., [4,15]).

2.3.1. Reaction Network

Our model assumed that sequential RD can occur for the entire reaction chain PCE→TCE→cis-DCE→VC, while oxidation (OX) is limited to cis-DCE and VC. Such assumptions are in agreement with the literature since clear evidence of RD was provided for all chloroethenes, while OX was extensively documented only for cis-DCE and VC, but rarely for TCE and PCE [30]. For a generic species "x", first-order degradation kinetics of the form

$$Rate_x = K_x C_x \quad (1)$$

were adopted for both RD and OX. In Equation (1), *Rate* is the degradation rate which represents the variation of concentration with time [M L^{-3} T^{-1}], K is the kinetic rate constant [T^{-1}] and C is the concentration [M L^{-3}]. During RD, one mole of the parent product (e.g., PCE) becomes one mole of the daughter product (e.g., TCE). The final products of cis-DCE and VC oxidation (CO_2 and Cl^-) were not included in the model.

To simulate carbon isotope fractionation, a bulk isotope model [15] was adopted. For each compound of the degradation chain, couples of "light" and "heavy" C isotope species were defined (i.e., "light" PCE and "heavy" PCE, "light" TCE and "heavy" TCE, etc.). Degradation rates were defined for all "heavy" and "light" species for each step of the reaction network. For instance, in the case of PCE, the degradation rate of the most abundant "light" species, namely, $PCE(l)$, was equal to

$$Rate_{PCE(l)} = K_{PCE}\, C_{PCE(l)} \quad (2)$$

where K_{PCE} is the first-order degradation constant for PCE and $C_{PCE(l)}$ is the concentration of $PCE(l)$. For the "heavy" species, namely, $PCE(h)$, the degradation rate was defined such that

$$Rate_{PCE(h)} = \alpha K_{PCE}\, C_{PCE(h)} \quad (3)$$

where α is the bulk fractionation factor of the reaction step [-] and $C_{PCE(h)}$ is the concentration of $PCE(h)$. The scalar factor α (fractionation factor) accounts for the slower reaction rate of the heavy species compared with the light one, which is usually expressed as an isotopic enrichment factor (ε) as follows:

$$\varepsilon = 1000(\alpha - 1) \quad (4)$$

The concentration of each of the two isotope species is then recalculated over a specified time interval by multiplying each of the degradation rate expressions (Equations (2) and (3)) by the interval length. The interval is imposed by the user and is calculated based on the distance traveled by water and its velocity.

The isotopic composition of the species is then computed using

$$\delta^{13}C_{PCE} = \left(\frac{R_{PCE}}{R_{standard}} - 1\right) \times 1000 \quad (5)$$

where $\delta^{13}C$ is the "delta" notation conventionally used to specify isotopic compositions [‰], R_{PCE} is the ratio between $PCE(h)$ and $PCE(l)$, and $R_{standard}$ is the ratio between ^{13}C and ^{12}C in the standard, which is known [31].

The whole approach (Equations (2)–(5)) was repeated to compute the $\delta^{13}C$ of the other "daughter" compounds formed from the dechlorination of PCE. The minimum, mean and maximum k and ε values for each compound obtained through a literature review are shown in Table 1. k_{RD} values were obtained from the compilation of [32], who considered bioremediation under monitored natural attenuation (MNA) field conditions. k_{OX} values were obtained from the compilation of [33]. ε_{OX} and k_{OX} for PCE and TCE were not considered in this study. ε values were obtained from two databases [4,34]. Further information can be found in the Supplementary Materials.

Table 1. Statistics of the enrichment factors (ε) and first-order degradation constants (k) obtained through a literature review. All ε values are expressed as "per mille" (‰).

	PCE	TCE	Cis-DCE	VC
		Reductive Dechlorination (RD)		
ε_{RD} min (‰)	−7.12	−16.40	−30.50	−28.80
ε_{RD} mean (‰)	−4.51	−11.65	−21.43	−24.52
ε_{RD} max (‰)	−1.60	−3.30	−14.90	−19.90
k_{RD} min (y^{-1})	0.00	0.00	0.00	0.00
k_{RD} mean (y^{-1})	1.07	1.10	1.82	2.20
k_{RD} max (y^{-1})	29.00	8.40	28.00	3.00
		Oxidation (OX)		
ε_{OX} min (‰)			−19.90	−8.20
ε_{OX} mean (‰)			−7.99	−6.06
ε_{OX} max (‰)			−0.90	−3.20
k_{OX} min (y^{-1})			102.57	15.70
k_{OX} mean (y^{-1})			323.03	43.80
k_{OX} max (y^{-1})			715.40	204.40

2.3.2. Reactive Transport Model

The reaction network described above was embedded into a 1-D transport model, which reproduced an L = 224 m long flow path, discretized into 28 regular cells that were 8 m wide. L covers the linear distance between the piezometers Pz22 (close to the landfill) and AEext4 (close to the ARLC), crossing the AN and AE biobarriers. The total simulation time was set to approximately 11 years in order to reach steady-state conditions. A summary of the model parameters is reported in Table 2.

Table 2. PHREEQC model input parameters. TOC: total organic carbon.

Parameter	Value	Unit
Domain length (L)	224	m
Tracer velocity (v_{nr})	0.45	m d^{-1}
Averaged chloroethene velocity (v_r)	0.10	m d^{-1}
Longitudinal dispersivity (α_L)	22.4	m
Cell length (ΔX)	8	m
Number of cells	28	-
Shifts	50	-
Time step length	80	d
Equivalent simulation time	4000	d
Cell numbers for reactive zone 1	1–7	-
Cell numbers for reactive zone 2	8–21	-
Cell numbers for reactive zone 3	22–28	-
Flow inlet/outlet boundary conditions	Constant flux	-
Bulk density (ρ_b)	1.6	g cm^{-3}
Porosity (ϕ)	0.25	-
Fraction of organic carbon (f_{oc})	10% of TOC	-

Aquifer properties were considered homogeneous in the modeled domain. The advective velocity for a conservative (i.e., a non-reactive) tracer (v_{nr}) was set to $v_{nr} = 0.45$ m/d. This value was derived from the already-interpreted results of a fluorescein dye tracer test performed at the site and reported in technical documents provided by the site's owner. The tracer test velocity agreed with the $v_{nr} = 0.37$–0.48 m/d obtained through the monitored groundwater head levels, assuming a hydraulic conductivity K = 14 m/d (obtained from slug tests performed on the site) and a porosity ϕ = 0.25 (typical value obtained from the literature for this type of aquifer [35] Following [36], we set a coefficient of longitudinal dispersivity $\alpha_L = 0.1L$, resulting in $\alpha_L = 22.4$ m.

Compared with a conservative tracer, the advective velocity of the reactive chloroethenes (v_r) was reduced by the effect of sorption on the porous medium. Thus, the pore water velocity in the model was set as the retarded velocity v_r and computed using

$$v_r = \frac{v_{nr}}{\overline{\beta}} \tag{6}$$

where $\overline{\beta}$ is the average retardation factor calculated from the species-specific retardation factors β_x, which are in turn calculated using (e.g., [37])

$$\beta_x = 1 + \frac{\rho_b}{\phi} K'_{d(x)} \tag{7}$$

where ρ_b is the bulk density of the soil [M L^{-3}] and K'_d is the distribution coefficient of the species x. The term K'_d can be calculated using

$$K'_d = f_{oc} k_{oc} \tag{8}$$

where f_{oc} is the fraction of organic carbon [-] and the species-specific k_{oc} is the partition coefficient between organic carbon and water [L^3 M^{-1}]. We used representative values for ρ_b and ϕ for silty sands and sandy silts, while we set $f_{oc} = 1\%$, which was a value obtained by considering one-tenth of the total organic carbon (TOC) measured in samples collected in the field and estimated as TOC = 10% (v/v) [38]. Typical values for k_{oc} were obtained from the Italian reference database for environmental health risk analysis [39]. The resulting k_{oc} and β values are listed in Table 3.

Table 3. Representative value of the partition coefficient between organic carbon and water (k_{oc}) and retardation factors (β) for chloroethenes. $\overline{\beta}$ is the average retardation factor.

Chloroethene	k_{oc} (cm^3/g)	β	$\overline{\beta}$
PCE	94.94	7.08	4.47
TCE	60.70	4.88	
Cis-DCE	39.60	3.53	
VC	21.73	2.39	

As direct information regarding the composition of the landfill was missing, the flow and solute input boundary condition was calculated from the groundwater composition at Pz22, i.e., the closest piezometer to the landfill (Figure 1). The source released a constant concentration of "light" and "heavy" PCE, TCE, cis-DCE and VC. The model concentrations of light and heavy species for each chloroethene are reported in Table 4. These values were calculated from the total concentrations and carbon isotopic ratios measured at Pz22 in May 2021, which are also reported in Table 4 and the "Results" section.

Table 4. Concentrations and isotopic compositions used to model the plume source in the PHREEQC model.

Compound	Concentrations (μM)	$\delta^{13}C$ (‰)
PCE tot	34.982	
PCE(l)	34.615	-58.2 ± 0.7
PCE(h)	0.367	
TCE tot	228.137	
TCE(l)	225.726	-49.7 ± 0.3
TCE(h)	2.411	
Cis-DCE tot	194.845	
Cis-DCE(l)	192.767	-40.3 ± 0.2
Cis-DCE(h)	2.078	
VC tot	1568.000	
VC(l)	1551.135	-32.7 ± 0.1
VC(h)	16.865	

The model assumed three different "reactive zones" (RZs; Figure 1c) by considering the different biodegradation processes and the corresponding degradation kinetics expected in the different portions of the flow path. Specifically, we defined the following:

1. Reactive zone 1 (RZ1), including model cells 1–7 and parametrized by k_{RD1} and ε_{RD1}. It represented the portion of the flow path immediately upgradient of the AN barrier, from Pz22 to between Pz13 and Pz10, where the AN barrier was located. Here, only natural RD was expected to take place without stimulation by the AN barrier.
2. Reactive zone 2 (RZ2), including cells 8–21 and parametrized by k_{RD2} and ε_{RD2}. It represented the portion of the flow path located between the AN and AE barriers until just upgradient of the piezometer 206S. Stimulated RD was expected to take place in this section of the flow path.
3. Reaction zone 3 (RZ3), including cells 22–28 and parametrized by k_{OX} and ε_{OX}. It represented the last portion of the flow path extending from 206S to the end of the transect, which included the AE barrier and piezometer AEext4 just downgradient of it. OX was expected to be largely stimulated by the AE barrier, while RD was not expected to be as efficient as in the upgradient zones.

2.3.3. Model Calibration

Model calibration was carried out with a trial-and-error approach using the results of the May 2021 campaign, which provided a complete dataset for both concentrations and isotopic data. The weighted root-mean-square error ($wRMSE$) between the simulated and observed values was used as the error metric to obtain the best-fitting model parameters. For each species, $wRMSE$ was calculated using

$$wRMSE = \frac{1}{N}\sqrt{\sum_{i=1}^{N}\left[w_i\left(Y_{obs_i} - Y_{sim_i}\right)\right]^2} \quad (9)$$

where Y_{obs} is either the observed concentration or $\delta^{13}C$, Y_{sim} is either the simulated concentration or $\delta^{13}C$, w is an observation-specific weight and N is the number of observations ($i = 1, \ldots, N$).

A total of 16 parameters were estimated during the calibration. Specifically, we estimated the three RD parameters (k_{RD1}, k_{RD2}, ε_{RD}) for each of the four considered species (PCE, TCE, cis-DCE and VC) and the two OX parameters (k_{OX}, ε_{OX}) for cis-DCE and VC.

Two different calibration approaches were used. In the first approach ("Approach 1"), we initially calibrated the degradation rate constants (k_{RD1}, k_{RD2}, k_{OX}) by matching the concentration data. Then, we used the best-fitted k to obtain the enrichment factors

(ε_{RD1}, ε_{RD2}, ε_{OX}) by matching the isotopic data. In "Approach 1", we assigned a weight $w = 1$ to all observations by considering that all observations were equally reliable.

Calibrated parameters using "Approach 1" could be affected by two problems. First, no constraints on the best-fit ε were imposed. This may lead to unrealistic enrichment factors when compared with the typical values reported in the literature (Table 1). Second, the third reaction zone covered 206S and AEext4. Concentrations at these piezometers may not have exclusively depended on OX processes, but also depend on the RD processes that took place in reactive zones RZ1 and RZ2. As such, the use of concentrations and isotopic compositions at 206s and AEext4 for the estimation of k_{OX} and ε_{OX} were expected to be more uncertain than the use of concentrations and isotopic compositions at the other piezometers for the estimation of $k_{RD1,2}$ and $\varepsilon_{RD1,2}$. To account for the possible problems with "Approach 1", the second calibration approach ("Approach 2") adopted a different strategy. For the reaction zones RZ1 and RZ2, the degradation rate constants k_{RD} were calibrated by simultaneously matching concentration and isotopic data, and prioritizing the minimization of RMSE of isotopic data rather than concentrations. The maximum and minimum ε_{RD} values were constrained within the ranges indicated in Table 1. For RZ3, k_{OX} was estimated exclusively using the CSIA data. We fixed ε_{OX} according to the average, minimum and maximum values obtained from the literature. For each ε_{OX} value, we fitted the isotopic data by changing k_{OX} values within the ranges indicated in Table 1. To account for the uncertainty in the observations, in "Approach 2", we assigned $w = 0.5$ to the CSIA data in AExt4 for PCE and TCE, lacking information at 206S, and to cis-DCE and VC in RZ3, to account for the more uncertain use of piezometers 206S and AEext4 for the estimation of k_{OX} and ε_{OX}. For all other observations $w = 1$.

A sensitivity analysis was conducted to evaluate the impact of the variation of α_L and the best-fitted k_{RD2} and ε_{RD} obtained using "Approach 2". The results did not provide further insight into the interpretation of the processes and are reported in the Supplementary Materials.

3. Results

3.1. Hydrochemical and Isotopic Analyses

3.1.1. Concentration Data

Figure 2 shows the statistics, in the form of boxplots, of all concentration time series that were obtained by merging the 33 available monitoring campaigns from May 2016 to January 2022. The time series of the individual sampling campaigns can be found in the Supplementary Materials. All horizontal axes in the plots report the distance from Pz22.

A first key observation was that while RD positively affected the biodegradation of all species, RD was less efficient for cis-DCE and VC than for PCE and TCE. Upgradient of the AN barrier (i.e., from Pz22 and Pz13), Figure 2 shows that the concentrations of PCE remained constant with a median value close to 6000 µg/L, while an increase in concentrations was observed for TCE, cis-DCE and VC. Across the AN barrier (i.e., between Pz13 and Pz10), the PCE and TCE concentrations dropped from 6300 µg/L to 470 µg/L (i.e., decreased by 92.6%) and from 50,500 µg/L to 1500 µg/L (i.e., a decrease of 97.1%), respectively. Furthermore, the cis-DCE and VC concentrations considerably decreased from 36,000 µg/L to 9000 µg/L (i.e., 75%) and from 149,000 µg/L to 55,000 µg/L (i.e., 73.1%), respectively.

Moving downgradient of the AN barrier and approaching the AE barrier, the overall degradation efficiency jumped to >99.9% for PCE, TCE and cis-DCE and to 84–91.8% for VC. At 206S, we observed further decreases in PCE to 0.80 µg/L, TCE to 2.80 µg/L, cis-DCE to 0.71 µg/L and VC to 12,200 µg/L. At AEext4, we found median values of 1.39 µg/L for PCE, 11.00 µg/L for TCE, 7.55 µg/L for cis-DCE and 24,050 µg/L for VC. This meant that the sequential ISB was highly beneficial for the removal of contaminant mass from the aquifer.

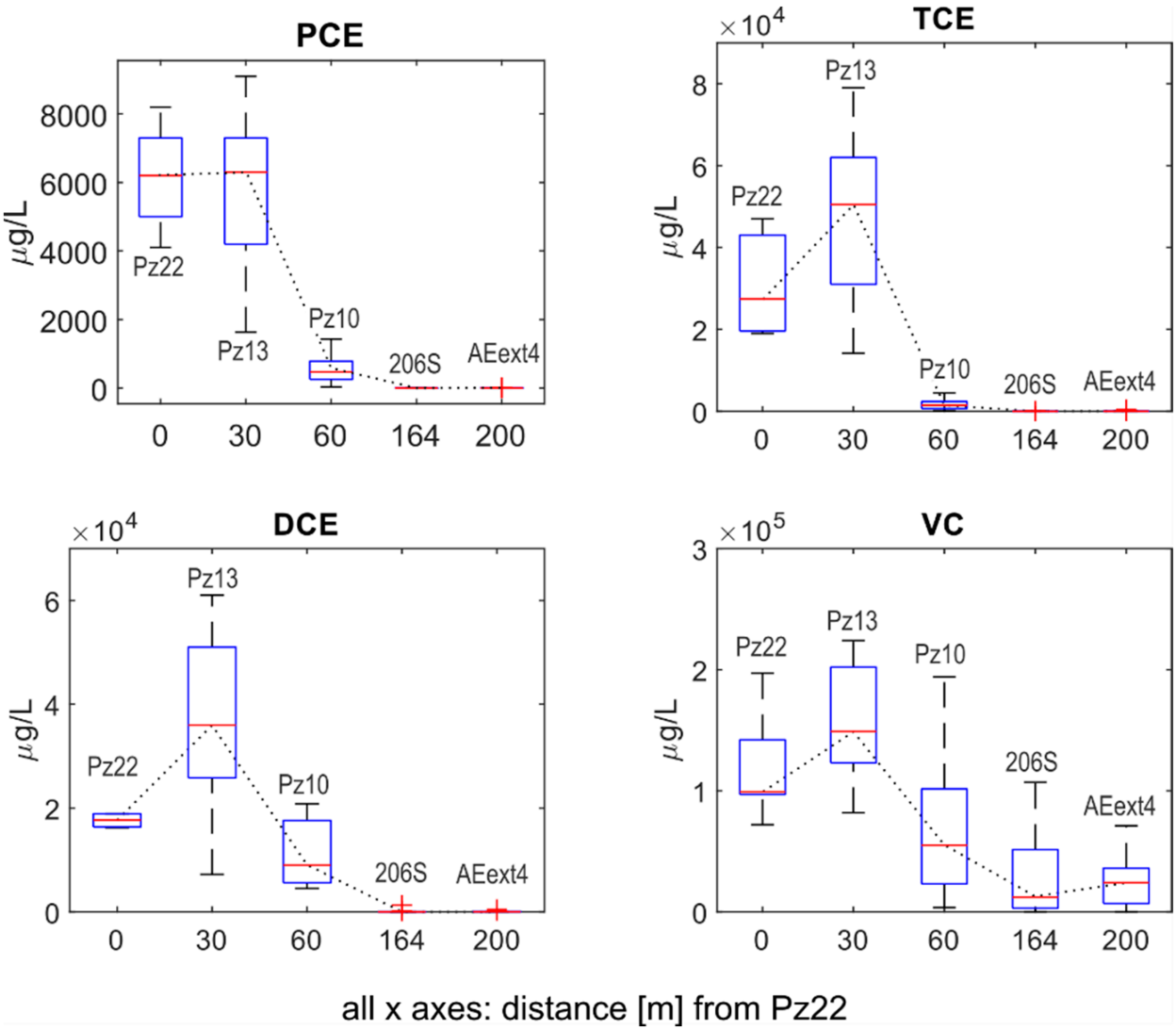

Figure 2. Evolution of the PCE, TCE, DCE and VC concentrations along the transect from Pz22 to AEext4 for all available sampling campaigns. The dotted black line connects the median values (red marks) of the different boxplots.

3.1.2. Environmental Parameters

Trends of chloroethene concentrations were consistent with the variations in Eh, iron, manganese, sulfate and ammonium concentrations measured in the boreholes. Statistics for Eh, iron, manganese, sulfate and ammonium concentrations are shown as boxplots in Figure 3. The individual time series for each monitoring campaign can be found in the Supplementary Materials. Data for pH, electrical conductivity and temperature were not reported, as no spatiotemporal trends or remarkable seasonal variations were observed for these parameters.

Upgradient of the AN barrier (from Pz22 to Pz13), the Eh value decreased from −139 mV to −181 mV, while at Pz10, just downgradient of the AN barrier, a value as low as −255 mV was reached as a consequence of the injection of the reducing substrate. The decrease in Eh between Pz22 and Pz13 suggested that while the injection rates at the AN barrier were very modest, the resulting radially divergent flow could have forced injected solute to move locally upgradient and against the mean natural gradient of the aquifer.

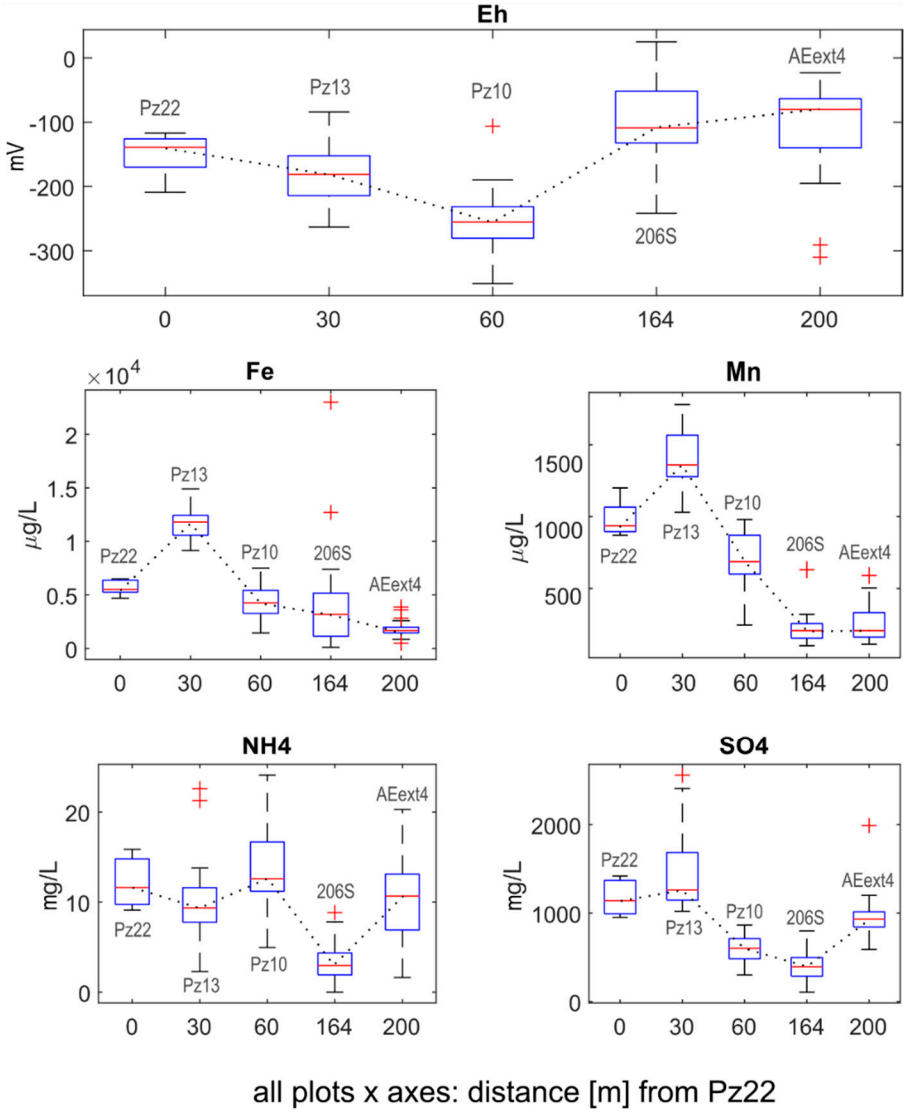

Figure 3. Evolution of the oxidizing–reduction potential (expressed as Eh), iron, manganese, ammonium and sulfate concentrations along the transect from Pz22 to AEext4 for all available sampling campaigns. The dotted black line connects the median values (red marks) of the different boxplots.

Between Pz22 and Pz13, we observed an increase in median concentrations of Fe (from 5500 µg/L to 11,800 µg/L) and Mn (from 935 µg/L to 1360 µg/L). This trend was consistent with the decrease in Eh, which could mobilize Fe and Mn by dissolving iron- and manganese hydroxides. The decrease in Fe and Mn concentrations from Pz13 to Pz10 (from 11,800 µg/L to 4255 µg/L for Fe and from 1360 µg/L to 686 µg/L for Mn) could be explained by the precipitation of Fe and Mn sulfides due to the presence of hydrogen sulfide produced by sulfate reduction [40–43], as observed for Eh < −200 mV in similar geological settings [44]. Indeed, SO_4 concentrations remained relatively stable between Pz22 and Pz13, while they decreased significantly between Pz13 and Pz10, reaching a value as low as 602 mg/L. This further confirmed that sulfate-reducing conditions were reached at the AN barrier.

Approaching the AE barrier, the Eh switched back to more oxidizing conditions (−109 mV in 206S and −80 mV in AEext4). Consistently, at 206S and AEext4, iron (3180 µg/L and 1670 µg/L, respectively) and manganese (206 µg/L in both piezometers) concentrations decreased compared with upgradient piezometers. In contrast, SO_4 concentrations were not as easily correlated with Eh variations in 206S. In fact, from Pz10 to 206S, SO_4 decreased while Eh increased. In contrast, from 206S to AEext4, SO_4 increased

from 395 mg/L to 931 mg/L, while Eh increased slightly. This latter trend could be due to sulfide oxidation due to more oxidizing conditions created at the AE barrier. This should have caused an increase in Fe and Mn concentrations as well, which may have been counterbalanced by the precipitation of Fe and Mn oxides/hydroxides, which are more stable compared with sulfides for Eh > −100 mV [44].

The behavior of NH_4 was more complex than the other species, yet it was still consistent with the general behavior of the sequential ISB system. In all boreholes, ammonium concentrations were well above the analytical detection limit (0.1 mg/L), which was expected for an aquifer with a high TOC (10% (*v*/*v*)). Upgradient from the AN barrier, from Pz22 to Pz13, the ammonium concentrations decreased from 11.62 mg/L to 9.35 mg/L, probably due to the decrease in the natural organic matter content in sediments caused by its progressive consumption during reductive processes, as observed in adjacent sites [45]. Concentrations of NH_4 increased again to 12.6 mg/L as a result of the injection of the reducing organic substrate at the AN barrier. The concentrations showed a significant drop at 206S (2.96 mg/L), consistent with the increasing distance from the injection wells and the associated lower availability of ammonium-producing substrate From 206S to AEext4; the concentrations then increased again (10.67 mg/L) due to the injection of nutrients (P and N) at the AE barrier.

3.1.3. C-CSIA Data

The C-CSIAs carried out in January and May 2021 were critical for providing key information regarding the biodegradation processes that occurred in the sequential ISB. The results are reported in Table 5. PCE and TCE isotopic signatures could not be determined in piezometer 206S, as the concentrations of these two compounds were below the detection limit for isotope analysis. Moreover, concentration data at Pz22 were not available for January 2021.

Table 5. Results from the C-CSIAs from samples collected in January and May 2021. * b.d.l.—below detection limit. The standard deviation of the concentration data was 35%.

	Pz22		**Pz13**		**Pz10**		**206s**		**AEext4**	
	Conc (µg/L)	**$\delta^{13}C$ (‰)**	**Conc (µg/L)**	**$\delta^{13}C$ (‰)**	**Conc (µg/L)**	**$\delta^{13}C$ (‰)**	**Conc (µg/L)**	**$\delta^{13}C$ (‰)**	**Conc (µg/L)**	**$\delta^{13}C$ (‰)**
January 2021										
PCE	/	−58.2 ± 0.7	/	/	1340	−55.2 ± 0.5	0.091	b.d.l. *	1.94	−42.3 ± 0.1
TCE	/	−49.7 ± 0.3	/	/	2250	−47.3 ± 0.1	0.41	b.d.l. *	8.1	−38.8 ± 0.6
Cis-DCE	/	−40.3 ± 0.2	/	/	17,600	−37.8 ± 0.2	0.71	−26.4 ± 0.4	232	−11.5 ± 0.5
VC	/	−32.7 ± 0.1	/	/	108,000	−32.9 ± 0.2	5200	−24.4 ± 0.1	8000	−23.2 ± 0.1
May 2021										
PCE	5800	−57.2 ± 0.3	3200	−55.7 ± 0.1	1410	−55.8 ± 0.4	0.054	/	0.94	−23.0 ± 0.5
TCE	30,000	−49.4 ± 0.2	20,700	−49.3 ± 0.3	4400	−47.4 ± 0.4	0.122	/	3.00	−32.1 ± 0.7
Cis-DCE	18,900	−40.6 ± 0.5	30,600	−46.7 ± 0.1	17,800	−38.9 ± 0.5	0.5	−31.6 ± 0.8	490	−18.7 ± 0.5
VC	98,000	−32.4 ± 0.3	125,000	−33.1 ± 0.2	121,000	−33.2 ± 0.1	590	−42.5 ± 0.2	5800	−28.0 ± 0.1

For each compound, the variation in $\delta^{13}C$ along the flow path in January and May 2021 is displayed in Figure 4.

The results revealed a general progressive increase in $\delta^{13}C$ for all chloroethenes from Pz22 to AEext4 in both sampling campaigns, which was consistent with the isotopic enrichment caused by degradation processes. In fact, during degradation, microbes tend to favor isotopically lighter molecules (containing ^{12}C) rather than heavier molecules containing one or more heavy atoms (^{13}C). This leads to an enrichment of heavier molecules in the remaining contaminant, which translates into an increase of its $\delta^{13}C$.

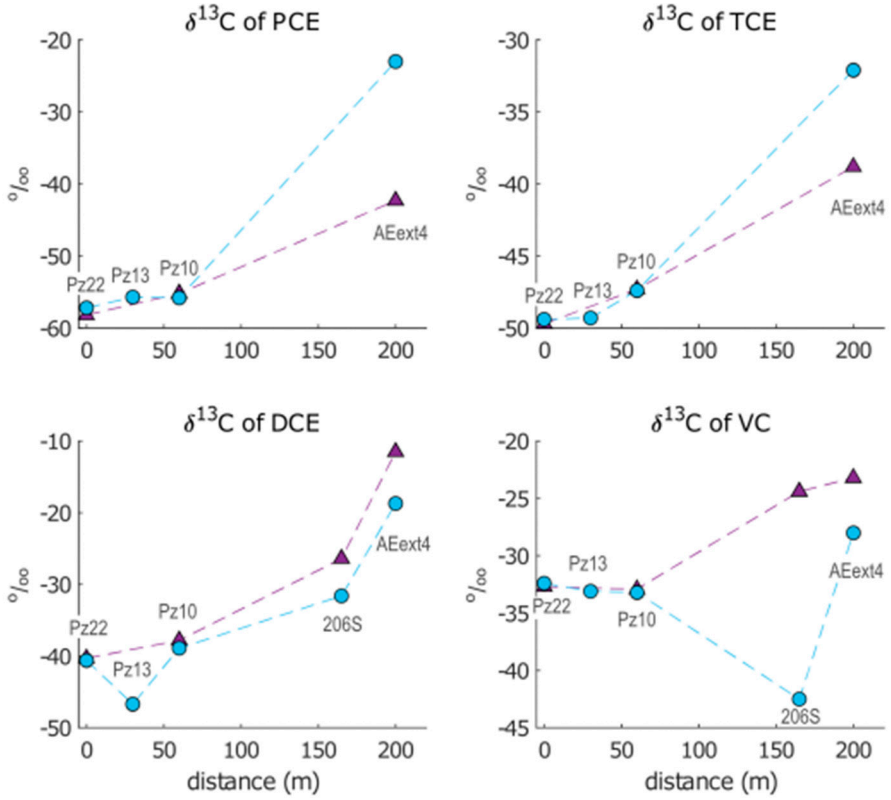

Figure 4. Evolution of isotopic signatures for PCE, TCE, cis-DCE and VC in January 2021 (purple triangles) and May 2021 (blue circles) from Pz22.

The isotopic enrichment produced along the AN barrier from Pz22 to Pz10 was similar in both sampling campaigns for all compounds. Instead, higher temporal variations in isotopic compositions were observed downgradient of Pz10.

Isotopic shifts ($\Delta^{13}C$) were calculated for each compound as the difference between $\delta^{13}C$ in the downgradient piezometer and $\delta^{13}C$ in the respective upgradient piezometer. All isotopic shifts can be found in the Supplementary Materials (Table S4). The isotopic enrichment of PCE and TCE from Pz10 to AEext4 was higher in May ($\Delta^{13}C_{PCE}$ = 32.8‰ and $\Delta^{13}C_{TCE}$ = 15.3‰) compared with January ($\Delta^{13}C_{PCE}$ = 12.9‰ and $\Delta^{13}C_{TCE}$ = 8.5‰). Opposite behavior was observed for cis-DCE, as a slightly higher enrichment was measured in January from Pz10 to 206S ($\Delta^{13}C_{DCE}$ = 11.4‰) and from 206S to AEext4 ($\Delta^{13}C_{DCE}$ = 14.9‰) than in May ($\Delta^{13}C_{DCE}$ = 7.4‰ from Pz10 to 206S and $\Delta^{13}C_{DCE}$ = 12.9‰ from 206S to AEext4). For VC, the isotopic composition also increased monotonically from Pz22 to AEext4 in the January dataset. In contrast, in May, we found a negative isotopic shift from Pz10 to 206S ($\Delta^{13}C_{VC}$ = −9.3‰), followed by a significant enrichment from 206S to AEext4 ($\Delta^{13}C_{VC}$ = 14.5‰). However, the final isotopic composition in AEext4 in May ($\delta^{13}C$ = −28.0‰) did not reach values as high as in January ($\delta^{13}C$ = −23.2‰). The unexpected drop in $\delta^{13}C_{VC}$ measured in May 2021 points to a likely intervention of processes different from biodegradation on the isotopic signature of VC, such as volatilization, dilution or mixing of multiple flow paths, as addressed in the "Discussion" section.

Overall, steady behavior was observed at the AN barrier between January and May, while significant differences were detected in the AE area. This points to major stability of the microbial activity in the AN zone compared with the AE zone, possibly due to the intervention of physical processes linked to the activity of the AE barrier, e.g., a local variation in air injection rates (possibly due to temporary malfunctioning of the AS wells). This is also in line with the hypothesis of the intervention of volatilization on the isotopic signature of VC in May since a higher injection rate of AS wells could lead to its volatilization.

3.2. Geochemical Model

The calibration process using both methods resulted in an excellent matching between observed and simulated concentration and isotopic data. However, the use of "Approach 1" generated best-fitted degradation constants falling within the ranges indicated in Table 1, but the enrichment factors were not consistent with literature values. In contrast, the use of "Approach 2" resulted in more consistency between enrichment factors obtained in the literature and those obtained from the model at the expense of a slightly poorer matching between measured and calculated concentrations.

3.2.1. Approach 1

A summary of the fitted ε and k values and the corresponding RMSEs for the concentration and CSIA data are reported in Table 6. The results of the concentration and isotopic data simulations are displayed in Figure 5.

Table 6. Calibrated k and ε values for the tested scenarios with May 2021 data.

	PCE	TCE	Cis-DCE	VC
Approach 1—Reductive Dechlorination (RD)				
k_{RD1} (y^{-1})	0.84	0.43	0.00	0.00
k_{RD2} (y^{-1})	2.70	11.00	2.15	0.48
ε_{RD} (‰)	−9.4	−3.6	−6.2	−2.0
Approach 1—Oxidation (OX)				
k_{OX} (y^{-1})	-	-	50	50
ε_{OX} (‰)	-	-	−2.2	−1.2
wRMSE				
Concentrations	0.07	0.60	16.60	159.50
CSIA	3.89	0.36	1.18	1.67
Approach 2—Reductive dechlorination (RD)				
k_{RD1} (y^{-1})	0.3	0.2	0	0
k_{RD2} (y^{-1})	6.5	2.9	0.6	0
ε_{RD} (‰)	−5.6	−5.7	−16.0	0
Approach 2—Oxidation (OX) *Using the Average [Minimum ÷ Maximum] ε_{OX}*				
k_{OX} (y^{-1})	-	-	4.7 [0.7 ÷ 155]	2.9 [1.7 ÷ 12.6]
ε_{OX} (‰)	-	-	−7.99 [−19.9 ÷ −0.9]	−6.06 [−8.2 ÷ −3.2]
wRMSE (average ε_{OX})				
Concentrations	1.10	13.14	24.08	157.76
CSIA	1.88	0.13	1.12	0.80

The best-fitted RD degradation rates for each reaction zone (RZ) were k_{RD1} = 0.84 y^{-1} and k_{RD2} = 2.70 y^{-1} for PCE and k_{RD1} = 0.43 y^{-1} and k_{RD2} = 11.00 y^{-1} for TCE. The larger degradation rate for TCE in RZ2 was explained by the steep drop in concentrations observed from Pz13 to Pz10 (from approximately 160 µM to approximately 35 µM). For cis-DCE, the best-fitting parameters were k_{RD1} = 0 and k_{RD2} = 2.15 y^{-1}. The model reproduced the accumulation of cis-DCE at Pz13 and the calculated value still fell within the standard deviation of the observed data. The fitted $k_{RD1} = 0$ was consistent with the lack of cis-DCE degradation expected in the anaerobic reaction zone RZ1 upgradient of the AN barrier. A large deviation was present between the observed and simulated concentrations in 206S, as the calculated values were three orders of magnitude higher (6 µM) than the observed values (0.005 µM). For VC, the best-fitted parameters were k_{RD1} = 0 and k_{RD2} = 0.48 y^{-1}. As in the case of cis-DCE, the fitted k_{RD1} agreed with the expected lack of VC degradation upgradient of the AN barrier, and the calculated VC concentrations fell within the standard deviations of observed data for Pz13 and Pz10. However, the

calculated concentrations at 206S were close to 400 µM, which was about 40 times higher than the observed concentrations (9.44 µM). The best-fitted OX degradation kinetics k_{OX} were 50 y^{-1} for both cis-DCE and VC. Such markedly higher values compared with the RD kinetic rates agreed with the literature data (Table 1).

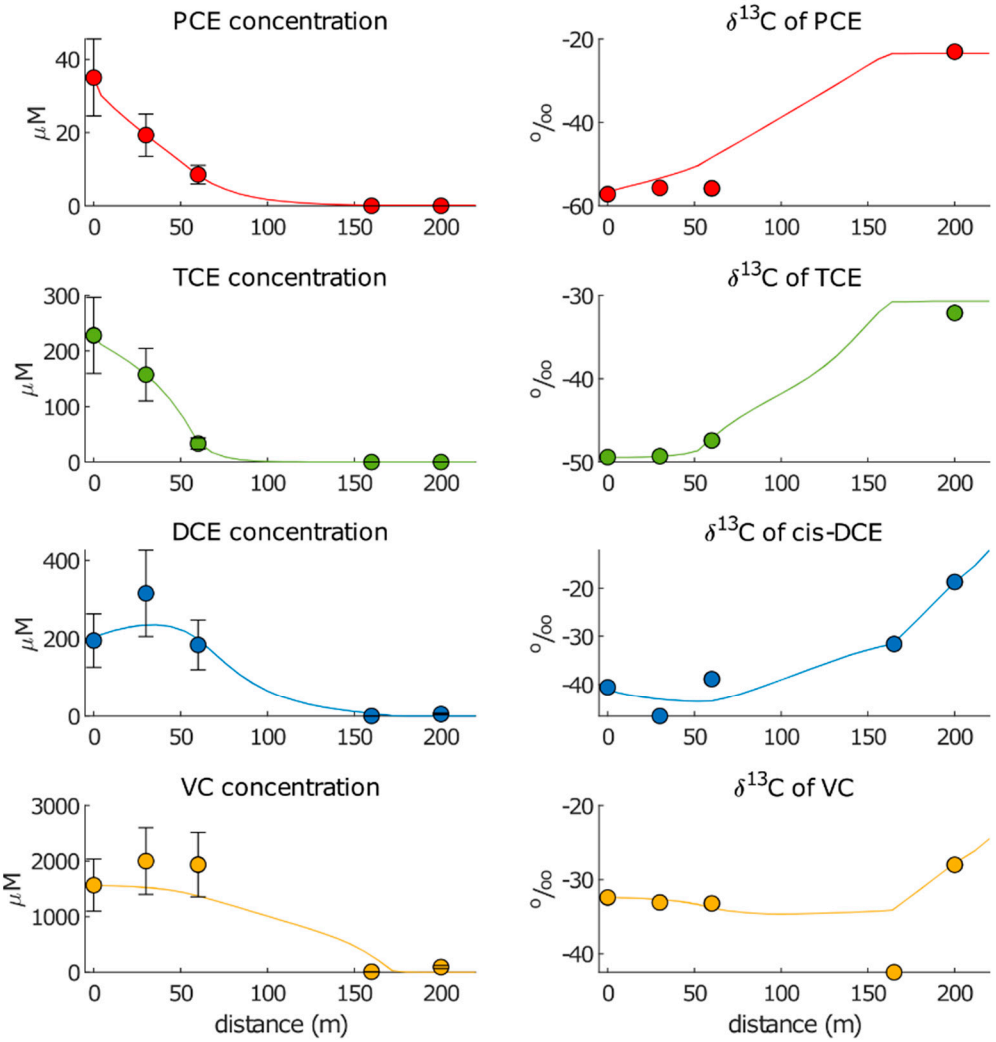

Figure 5. Simulated (lines) and observed (dots) chloroethenes concentrations and isotopic compositions using the first calibration ("Approach 1").

Considering the best-fitted k_{RD} and k_{OX}, the lowest wRMSE were calculated for the PCE and TCE concentrations (equal to 0.07 and 0.60, respectively), for which the concentration data were perfectly reproduced. Higher wRMSE were obtained for DCE (16.60) and VC (159.50) concentrations, for which the model did not allow for accurately reproducing the accumulation of both compounds at Pz13, as well as the observed concentrations in 206S. As for isotopic data, the resulting wRMSEs were the lowest for TCE (0.36), highest for PCE (3.89) and cis-DCE and VC fell in between (1.18 and 1.67, respectively). Notwithstanding the general good reproduction of isotopic evolutions, the enrichment factors calculated using "Approach 1" fell outside of the literature ranges, with a few exceptions. The resulting ε_{RD} values were −9.4‰ for PCE (literature range is −7.12–−1.60‰), −3.6‰ for TCE (literature range is −11.65–−3.30‰), −6.2‰ for cis-DCE (literature range is −30.50–−14.90‰) and −2.0‰ for VC (literature range is −28.8–−19.9‰). The resulting ε_{OX} values were −2.2‰ for cis-DCE (−7.90–−0.90‰) and −1.2‰ for VC (−6.06–−3.20‰). This suggested that "Approach 1" was not useful for estimating the bioremediation parameters.

3.2.2. Approach 2

Best-fitted concentration and isotopic data are displayed in Figure 6, while the summary of the results can be found in Table 6.

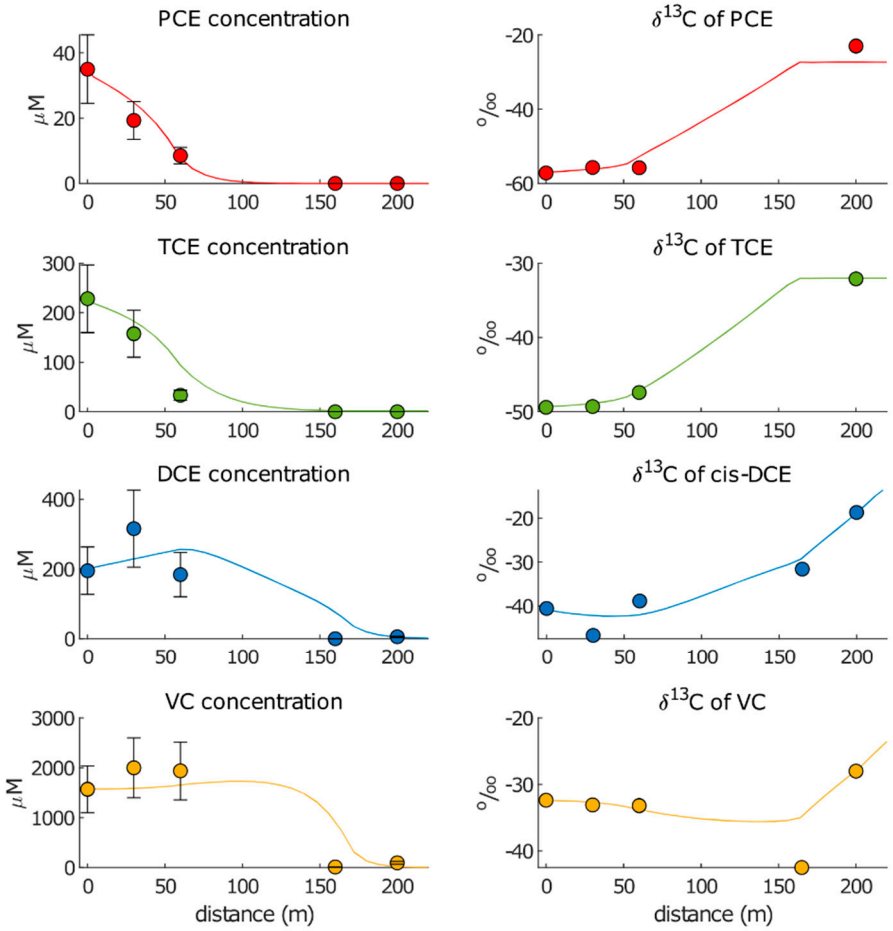

Figure 6. Simulated (lines) and observed (dots) showing the chloroethene concentrations and isotopic compositions in "Approach 2".

For cis-DCE, a much lower k_{RD2} (0.6 y^{-1}) was found compared with "Approach 1", while the resulting enrichment factor (−16.0‰) fell within the literature range. The lower k_{RD2} for cis-DCE combined with the lower k_{RD1} and higher k_{RD2} of TCE (which generated less production of cis-DCE upgradient and more production downgradient of the AN barrier) caused an increase in the concentration peak, which shifted toward Pz10, compared with the concentration peak obtained with "Approach 1".

The very low k_{RD2} for cis-DCE was explained by considering that this species is usually hardly degraded through RD. The same holds for VC, for which we obtained $k_{RD1} = k_{RD2} = 0$. The null degradation rate in both zones demonstrated that VC was possibly not degraded at all under anaerobic conditions at the site. The absence of VC concentration abatement from Pz22 to Pz10 was coherent with the small decrease in $\delta^{13}C_{VC}$ between the two points ($\Delta^{13}C = -0.8$‰), which resulted from the production of VC (from RD of cis-DCE) in the absence of its degradation.

For the estimation of the OX degradation rates, Table 6 compares the results from the calibration by fixing the average, minimum and maximum enrichment factors values reported in the literature (Table 1). We obtained great variability in the best-fitted oxidative rates, namely, k_{OX} = 0.7–155 y^{-1} for cis-DCE and k_{OX} = 1.7–12.6 y^{-1} for VC. These ranges agreed with the results obtained using "Approach 1" (k_{OX} = 50 y^{-1}). The much higher OX

rate obtained for these compounds compared with the RD rates further confirmed that aerobic biodegradation of cis-DCE and VC was more effective than anaerobic biodegradation.

In this case, overall higher wRMSEs for concentrations were obtained compared with "Approach 1", even though in "Approach 2", the weight of observations in RZ3 (206S and AEext4) were halved. Like in "Approach 1", increases in concentration wRMSEs from PCE to VC were observed, and the lowest and the highest wRMSEs for isotopic data were obtained for TCE (0.13) and PCE (1.88), respectively.

4. Discussion

4.1. Interpretation of the Fitted Parameters in "Approach 2"

The combination of C-CSIAs and their RTM-based interpretation provided a novel and unique way to quantify the biodegradation kinetics that occurred in the different parts of a sequential ISB.

The degradation of PCE and TCE occurred both upgradient (reactive zone RZ1) and downgradient (reactive zone RZ2) of the AN barrier. The higher degradation rates in RZ2 (k_{RD2} = 6.5 y^{-1} for PCE and k_{RD2} = 2.9 y^{-1} for TCE) compared with RZ1 (k_{RD1} = 0.3 y^{-1} for PCE and k_{RD1} = 0.2 y^{-1} for TCE) were explained considering the effect of the injected substrate in the AN barrier, proving its effectiveness in biostimulating the RD of higher chlorinated ethenes.

The fact that k_{RD} of PCE was higher than the k_{RD} of TCE was explained by considering that the degradation process tends to slow down for less chlorinated compounds [46–50]. Microorganisms such as *Dehalococcoides* and *Dehalobacter* preferentially undertake the RD of higher chlorinated ethenes due to the higher energetic yields associated with their reduction compared with the RD of lesser chlorinated ethenes [3,30].

Degradation rate constants for PCE and TCE upgradient of the AN barrier (k_{RD1}) were of the same order of magnitude as those reported in Table 1, which were obtained from the compilation by [51]. Note that these authors analyzed biodegradation in sites exclusively undergoing natural attenuation. The similarity of degradation rates between our study and that compilation suggested that dehalogenating bacteria in the study site were able to carry out an important process of degradation of higher chlorinated ethenes even without the addition of substrates. However, given the high contaminant concentrations, the process of natural attenuation was not enough to abate the concentrations of PCE and TCE to under a satisfactory level, as demonstrated by the high concentrations of both compounds at Pz13. Even though the k_{RD2} values were lower than the maximum values observed for natural attenuation at some sites (in particular for PCE, for which a maximum rate of 29.00 y^{-1} was observed), they were still much higher than the mean literature values [51].

C-CSIA data showed an important isotopic enrichment of TCE from Pz13 to AEext4. Since CSIA data in the middle borehole 206S for TCE were not available, uncertainties remain about how much of the observed isotopic enrichment was produced upgradient and downgradient of 206S through RD and OX, respectively. While TCE is preferably degraded through RD, a few studies reported its degradation under aerobic conditions [52–55]. However, we believe that TCE OX is much less effective than RD, as no specific aerobic microorganism specialized in TCE degradation has been found to date in the study area. If part of the observed TCE enrichment in AEext4 were produced by OX at the AE barrier, a lower ε_{RD} would be needed for TCE. This would result in a substantially lower calibrated ε_{RD} for TCE compared with PCE, which is not usually observed, since ε values for RD of chloroethenes by *Dehalococcoides* and *Dehalobacter* tend to decrease from the higher to the lower chlorinated compounds [46–50]. The same considerations apply to PCE. In this case, we could safely rule out aerobic degradation since evidence of this process in the literature is scarce [3,56].

Degradation of cis-DCE and VC was more efficient through OX rather than RD, as expected. The literature ε_{OX} values considered for these compounds spanned a huge range, thus the resulting k_{OX} values differed markedly (0.7–155 y^{-1} for cis-DCE and 1.7–12.6 y^{-1} for VC). However, even when using the lowest literature values for ε_{OX} (−19.9‰ for

cis-DCE and −8.3‰ for VC), a certain degree of degradation was produced nonetheless (0.9 y^{-1} and 1.5 y^{-1} for cis-DCE and VC, respectively). Moreover, VC degradation through OX was hugely underestimated since $\delta^{13}C_{VC}$ calculated in 206S by the model was higher than the actual value ($\Delta^{13}C$ = 7.5‰). This meant that the calibrated k_{OX} of VC reflected only part of the enrichment produced by OX through the AE barrier from 206S and AEext. Notwithstanding the uncertainty of the ε_{OX} values, the resulting k_{OX} showed that cis-DCE and VC degradation at the AE barrier was stimulated much more efficiently than in anaerobic conditions. However, the k_{OX} ranges for these two compounds comprised much lower values compared with the literature values (Table 1).

The slight increase in concentrations observed from 206S to AEext4 for all compounds could not be reproduced considering that only oxidation was active between these two piezometers, and thus, no daughter compound was produced via RD from 206S onward. This suggested that RD may continue even after the onset of OX at 206S. This would allow for producing TCE, cis-DCE and VC via RD, even at the AE barrier. However, the concentrations of PCE and TCE were not high enough to produce the increase observed for cis-DCE and VC concentrations, which would be even higher than observed, since cis-DCE and VC were simultaneously being degraded via oxidative pathways. Moreover, the same increase was observed for PCE, which is the parent compound. Thus, a more likely explanation might be that 206S did not lie perfectly on the hypothesized flow path.

4.2. Limitations and Future Developments

Although the use of C-CSIA and RTM was demonstrated to be critical to disentangle the processes that occurred at the site, the model could not reproduce the entire behavior of VC isotopic data. For instance, the model did not correctly simulate the marked drop in $\delta^{13}C$ observed in May 2021 at 206S (d = 164 m) (Figure 4). Future developments are envisioned to improve the understanding of the processes occurring at the study site and obtain more robust modeling tools that are able to make predictions about the fate of contaminants. Specifically, future studies shall consider the following limiting factors of the present work.

Processes not included in the reactive model. Our model assumed that biodegradation was the sole process that altered the chloroethene concentrations and isotopic composition. However, other processes, such as volatilization [57], could remove organic compounds from the aquifer and cause isotopic fractionation. Volatilization alters the isotopic fingerprint, reducing the $\delta^{13}C$ value while decreasing the concentrations of polluted groundwater. Since air sparging takes place at the AE barrier, volatilization could be invoked to explain the drop in VC concentration coupled with the huge decrease in $\delta^{13}C_{VC}$ observed from Pz10 to 206S. However, to the best of our knowledge, $\delta^{13}C$ depletion during volatilization was only demonstrated for TCE [58–60] and dichloromethane [58], but never for VC.

Use of first-order degradation rates. Our kinetic constants were calculated using a first-order model for which the rates depended linearly on the k value and the compound concentration (Equation 1). While the model provided excellent fitting of the observed data, there are many factors that could nonlinearly influence the degradation rates along a flow path. One of them is the presence of alternative terminal electron acceptors (TEAs), which can compete with chloroethenes for hydrogen produced by the fermentation of the organic substrate injected and the organic matter naturally present in the site [61,62]. Iron and sulfate are the most important TEAs to consider since they are present in very high concentrations at the study site [56–58]. The first-order model did not consider the so-called "Haldane inhibition", i.e., the inhibition of chloroethene RD due to its own concentration [62–65]. It also ignores the competition with higher chlorinated ethenes. In fact, higher chlorinated solvents are preferentially used as a source of energy, inhibiting the degradation of lesser chlorinated compounds [62,64,66–68].

Use of a one-dimensional reactive transport model. Our 1-D reactive transport model assumed that the flow path perfectly crossed the five boreholes analyzed in this work. However, this remained an approximation of the more complex and multidimensional

real-life aquifer system. Such a system is composed of multiple flow paths due to the presence of multiple boundary conditions (such as the multiple pumping wells injection and extracting air and water to the soil), and the ubiquitous presence of soil heterogeneity. For instance, concentrations and isotopic data at 206S may be affected by the mixing of different flow paths. This could explain the slight increase in concentrations observed from 206S to AEext4, which could not be reproduced by considering a single flow path, as discussed in Section 4.1.

Support from other isotopes. Our study was based on C-CSIA, which is widely adopted to study biodegradation processes in complex aquifers. However, other isotopes could be adopted to achieve a better comprehension of degradation processes, as well as a better assessment of the ISB efficiency. In this sense, the acquisition of chlorine CSIA data [55,67,68] could provide further information regarding the degradation pathways, as well as provide an additional constraint on the calibrated model parameters.

5. Conclusions

Compound-specific carbon isotope analysis (C-CSIA) data and geochemical models were used to evaluate the efficiency of an 800 m-long sequential ISB system in Italy. This system was installed for the clean-up of a solute plume that originated from a former landfill in Northern Italy. The combination of these different tools and methodologies is novel and helped to disentangle the complex, nonlinear processes that occurred at different parts of the contaminated aquifer. Specifically, it helped with evaluating and quantifying natural biodegradation and anaerobic and aerobic biostimulation enhancing reductive dechlorination (RD) and oxidation (OX).

The combined use of concentration and CSIA data, which were interpreted using a properly calibrated geochemical model, was critical to identifying the relative impact of the different processes taking place in the different portions of the analyzed flow path. The following conclusions were drawn from this study.

The temporal trends of the observed concentrations suggested that the sequential ISB system was highly effective at degrading chloroethenes. The median values of PCE, TCE and cis-DCE dropped by >99% and VC dropped by >80%. The sequential effects of anaerobic and aerobic biostimulation were consistent with the trends in Eh and redox-sensitive species (Fe, Mn, SO_4^{2-}, NH_4^+).

Natural biodegradation of PCE and TCE took place upgradient of the AN barrier. Here, first-order degradation rate constants that measured the efficiency of the RD (k_{RD}) were k_{RD1} = 0.3 y^{-1} and k_{RD1} = 0.2 y^{-1}, respectively. Although this demonstrated the ability of the indigenous microbial populations to carry out RD without the addition of stimulating substrates, natural biodegradation was inefficient at producing a significant reduction in PCE and TCE concentrations. The resulting reaction rate constants estimated from boreholes downgradient of the AN barrier (k_{RD2}) were higher (k_{RD2} = 6.5 y^{-1} for PCE and k_{RD2} = 2.9 y^{-1} for TCE) compared with those obtained upgradient of the AN barrier. This suggested that biostimulation was required to make RD effective for the degradation of higher chlorinated compounds. Nonetheless, the very low or null estimated k_{RD2} for cis-DCE and VC (k_{RD2} = 0.6 y^{-1} and k_{RD2} = 0, respectively) indicated that RD was insufficient to complete the dechlorination process, further supporting the need for the sequential ISB.

The degradation of cis-DCE and VC was better accomplished through OX, which was stimulated by the AE barrier. Indeed, first-order degradation rate constants measuring the efficiency of the OX (k_{OX}) were much higher (k_{OX} = 0.7–155 y^{-1} for cis-DCE and k_{OX} = 1.7–12.6 y^{-1} for VC) than the RD rates estimated for these species.

Supplementary Materials: The following supporting information can be downloaded from https://www.mdpi.com/article/10.3390/pollutants2040031/s1, References [4,36,69] are cited in the supplementary materials.

Author Contributions: Conceptualization: all authors. Methodology, validation and formal analysis: G.C. and D.P. Project administration and funding acquisition: M.M. and G.P.B. All authors have read and agreed to the published version of the manuscript.

Funding: This research was funded by INAIL (Istituto Nazionale per l'Assicurazione Contro gli Infortuni sul Lavoro—National Institute for Insurance against Accidents at Work) through Call INAIL-Bric 2019 (project ID: 52).

Institutional Review Board Statement: Not applicable.

Informed Consent Statement: Not applicable.

Data Availability Statement: All data used in this study are included in the main manuscript or as Supplementary Materials.

Acknowledgments: We acknowledge the useful suggestions and comments by the two anonymous Reviewers, which have helped improve the quality of the manuscript. The results here presented have been developed in the frame of the MIUR Project "Dipartimenti di Eccellenza 2017—Le Geoscienze per la societa': risorse e loro evoluzione".

Conflicts of Interest: The authors declare no conflict of interest.

Abbreviations

M	Unit of mass
L	Unit of length
T	Unit of time
CSIA	Compound-specific isotope analysis
ISB	In situ bioremediation
AN	Anaerobic
AE	Aerobic
PCE	Tetrachloroethene
TCE	Trichloroethene
DCE	Dichloroethene
VC	Vinyl chloride
RD	Reductive dechlorination
OX	Oxidation
ALRC	Artificial land reclamation canal
RZ	Reactive zone
k_{OX}	Degradation rate constant for OX
k_{RD}	Degradation rate constant for RD
α_{L}	Longitudinal dispersivity
ε	Enrichment factor
v_r	Retarded velocity
v_{nr}	Non-reactive velocity or tracer velocity
β	Retardation factor
$\overline{\beta}$	Average retardation factor
ρ_b	Bulk density
ϕ	Porosity
f_{oc}	Fraction of organic carbon
k_{oc}	Partition coefficient between organic carbon and water (L/kg or cm^3/g)
K'_d	Distribution coefficient (mg sorbed/kg solid)/(mg solute/L pore water) (L/kg or cm^3/g)

References

1. Devlin, J.F.; Katic, D.; Barker, J.F. In Situ Sequenced Bioremediation of Mixed Contaminants in Groundwater. *J. Contam. Hydrol.* **2004**, *69*, 233–261. [CrossRef]
2. Leeson, A.; Beevar, E.; Henry, B.; Fortenberry, J.; Coyle, C. *Principles and Practices of Enhanced Anaerobic Bioremediation of Chlorinated Solvents*; Naval Facilities Engineering Service Center: Port Hueneme, CA, USA, 2004.
3. Tiehm, A.; Schmidt, K.R. Sequential Anaerobic/Aerobic Biodegradation of Chloroethenes—Aspects of Field Application. *Curr. Opin. Biotechnol.* **2011**, *22*, 415–421. [CrossRef] [PubMed]
4. Antelmi, M.; Mazzon, P.; Höhener, P.; Marchesi, M.; Alberti, L. Evaluation of MNA in A Chlorinated Solvents-Contaminated Aquifer Using Reactive Transport Modeling Coupled with Isotopic Fractionation Analysis. *Water* **2021**, *13*, 2945. [CrossRef]
5. Thomas, J.M.; Ward, C.H. In Situ Biorestoration of Organic Contaminants in the Subsurface. *Environ. Sci. Technol.* **1989**, *23*, 760–766. [CrossRef]
6. Fralish, M.S.; Downs, J.W. Vinyl Chloride Toxicity. In *StatPearls*; StatPearls Publishing: Treasure Island, FL, USA, 2022.
7. Frascari, D.; Fraraccio, S.; Nocentini, M.; Pinelli, D. Aerobic/Anaerobic/Aerobic Sequenced Biodegradation of a Mixture of Chlorinated Ethenes, Ethanes and Methanes in Batch Bioreactors. *Bioresour. Technol.* **2013**, *128*, 479–486. [CrossRef]
8. Němeček, J.; Marková, K.; Špánek, R.; Antoš, V.; Kozubek, P.; Lhotský, O.; Černík, M. Hydrochemical Conditions for Aerobic/Anaerobic Biodegradation of Chlorinated Ethenes—A Multi-Site Assessment. *Water* **2020**, *12*, 322. [CrossRef]
9. Lai, A.; Aulenta, F.; Mingazzini, M.; Palumbo, M.T.; Papini, M.P.; Verdini, R.; Majone, M. Bioelectrochemical Approach for Reductive and Oxidative Dechlorination of Chlorinated Aliphatic Hydrocarbons (CAHs). *Chemosphere* **2017**, *169*, 351–360. [CrossRef]
10. Zheng, C.; Bennett, G.D. *Applied Contaminant Transport Modeling*, 2nd ed.; John Wiley & Sons: New York, NY, USA, 1997.
11. Varisco, S.; Beretta, G.P.; Raffaelli, L.; Raimondi, P.; Pedretti, D. Model-Based Analysis of the Link between Groundwater Table Rising and the Formation of Solute Plumes in a Shallow Stratified Aquifer. *Pollutants* **2021**, *1*, 66–86. [CrossRef]
12. Casasso, A.; Tosco, T.; Bianco, C.; Bucci, A.; Sethi, R. How Can We Make Pump and Treat Systems More Energetically Sustainable? *Water* **2019**, *12*, 67. [CrossRef]
13. Ciampi, P.; Esposito, C.; Petrageli Papini, M. Hydrogeochemical Model Supporting the Remediation Strategy of a Highly Contaminated Industrial Site. *Water* **2019**, *11*, 1371. [CrossRef]
14. Van Breukelen, B.M.; Thouement, H.A.A.; Stack, P.E.; Vanderford, M.; Philp, P.; Kuder, T. Modeling 3D-CSIA Data: Carbon, Chlorine, and Hydrogen Isotope Fractionation during Reductive Dechlorination of TCE to Ethene. *J. Contam. Hydrol.* **2017**, *204*, 79–89. [CrossRef] [PubMed]
15. Van Breukelen, B.M.; Hunkeler, D.; Volkering, F. Quantification of Sequential Chlorinated Ethene Degradation by Use of a Reactive Transport Model Incorporating Isotope Fractionation. *Environ. Sci. Technol.* **2005**, *39*, 4189–4197. [CrossRef] [PubMed]
16. Barajas-Rodriguez, F.J.; Murdoch, L.C.; Falta, R.W.; Freedman, D.L. Simulation of in Situ Biodegradation of 1,4-Dioxane under Metabolic and Cometabolic Conditions. *J. Contam. Hydrol.* **2019**, *223*, 103464. [CrossRef] [PubMed]
17. Liu, P.; Wang, G.; Shang, M.; Liu, M. Groundwater Nitrate Bioremediation Simulation of In Situ Horizontal Well by Microbial Denitrification Using PHREEQC. *Water. Air. Soil Pollut.* **2021**, *232*, 356. [CrossRef]
18. Steefel, C.I.; Appelo, C.a.J.; Arora, B.; Jacques, D.; Kalbacher, T.; Kolditz, O.; Lagneau, V.; Lichtner, P.C.; Mayer, K.U.; Meeussen, J.C.L.; et al. Reactive Transport Codes for Subsurface Environmental Simulation. *Comput. Geosci.* **2014**, *19*, 445–478. [CrossRef]
19. Appelo, C.A.J.; Postma, D. *Geochemistry, Groundwater and Pollution*; A.A. Balkema Publishers: London, UK, 2005.
20. Pooley, K.E.; Blessing, M.; Schmidt, T.C.; Haderlein, S.B.; MacQuarrie, K.T.B.; Prommer, H. Aerobic Biodegradation of Chlorinated Ethenes in a Fractured Bedrock Aquifer: Quantitative Assessment by Compound-Specific Isotope Analysis (CSIA) and Reactive Transport Modeling. *Environ. Sci. Technol.* **2009**, *43*, 7458–7464. [CrossRef]
21. Courbet, C.; Rivière, A.; Jeannottat, S.; Rinaldi, S.; Hunkeler, D.; Bendjoudi, H.; de Marsily, G. Complementing Approaches to Demonstrate Chlorinated Solvent Biodegradation in a Complex Pollution Plume: Mass Balance, PCR and Compound-Specific Stable Isotope Analysis. *J. Contam. Hydrol.* **2011**, *126*, 315–329. [CrossRef]
22. Casiraghi, G.; Pedretti, D.; Beretta, G.P.; Bertolini, M.; Bozzetto, G.; Cavalca, L.; Ferrari, L.; Masetti, M.; Terrenghi, J. Piloting Activities for the Design of a Large-Scale Biobarrier Involving In Situ Sequential Anaerobic–Aerobic Bioremediation of Organochlorides and Hydrocarbons. *Water. Air. Soil Pollut.* **2022**, *233*, 425. [CrossRef]
23. Dalla Libera, N.; Pedretti, D.; Tateo, F.; Mason, L.; Piccinini, L.; Fabbri, P. Conceptual Model of Arsenic Mobility in the Shallow Alluvial Aquifers near Venice (Italy) Elucidated through Machine Learning and Geochemical Modeling. *Water Resour. Res.* **2020**, *56*, e2019WR026234. [CrossRef]
24. Carraro, A.; Fabbri, P.; Giaretta, A.; Peruzzo, L.; Tateo, F.; Tellini, F. Effects of Redox Conditions on the Control of Arsenic Mobility in Shallow Alluvial Aquifers on the Venetian Plain (Italy). *Sci. Total Environ.* **2015**, *532*, 581–594. [CrossRef]
25. Beretta, G.P.; Terrenghi, J. Groundwater Flow in the Venice Lagoon and Remediation of the Porto Marghera Industrial Area (Italy). *Hydrogeol. J.* **2017**, *25*, 847–861. [CrossRef]
26. Holliger, C.; Wohlfarth, G.; Diekert, G. Reductive Dechlorination in the Energy Metabolism of Anaerobic Bacteria. *FEMS Microbiol. Rev.* **1998**, *22*, 383–398. [CrossRef]
27. Lee, I.-S.; Bae, J.-H.; Yang, Y.; McCarty, P.L. Simulated and Experimental Evaluation of Factors Affecting the Rate and Extent of Reductive Dehalogenation of Chloroethenes with Glucose. *J. Contam. Hydrol.* **2004**, *74*, 313–331. [CrossRef] [PubMed]

28. Bouwer, E.; Norris, R.; Hinchee, R.; Brown, R.A.; Semprini, L.; Wilson, J.T.; Kampbell, D.H.; Reinhard, M.; Borden, R.C.; Vogel, T.; et al. Bioremediation of Chlorinated Solvents Using Alternate Electron Acceptors. In *Hanbook Bioremediation*; CRC Press: Boca Raton, FL, USA, 1994; pp. 149–175.
29. Parkhurst, D.L.; Appelo, C.A.J. *Description of Input and Examples for PHREEQC Version 3—A Computer Program for Speciation, Batch-Reaction, One-Dimensional Transport, and Inverse Geochemical Calculations*; U.S. Geological Survey: Denver, CO, USA, 2013; p. 493.
30. Dolinová, I.; Štrojsová, M.; Černík, M.; Němeček, J.; Macháčková, J.; Ševců, A. Microbial Degradation of Chloroethenes: A Review. *Environ. Sci. Pollut. Res.* **2017**, *24*, 13262–13283. [CrossRef] [PubMed]
31. Craig, H. Isotopic Standards for Carbon and Oxygen and Correction Factors for Mass-Spectrometric Analysis of Carbon Dioxide. *Geochim. Cosmochim. Acta* **1957**, *12*, 133–149. [CrossRef]
32. Tillotson, J.M.; Borden, R.C. Rate and Extent of Chlorinated Ethene Removal at 37 ERD Sites. *J. Environ. Eng.* **2017**, *143*, 04017028. [CrossRef]
33. Suarez, M.P.; Rifai, H.S. Biodegradation Rates for Fuel Hydrocarbons and Chlorinated Solvents in Groundwater. *Bioremediat. J.* **1999**, *3*, 337–362. [CrossRef]
34. *ESTCP Project ER-201029. Environmental Security and Technology Certification Program, Arlington, Virginia*; Report; 2014; p. 244. Available online: https://clu-in.org/download/contaminantfocus/tce/ER-201029-User-Guide.pdf (accessed on 20 October 2022).
35. Domenico, P.; Schwartz, F.W. *Physical and Chemical Hydrogeology*; John Wiley & Sons, Inc.: Hoboken, NJ, USA, 1990; ISBN 978-0-471-59762-9.
36. Gelhar, L.W.; Welty, C.; Rehfeldt, K.R. A Critical Review of Data on Field-Scale Dispersion in Aquifers. *Water Resour. Res.* **1992**, *28*, 1955–1974. [CrossRef]
37. Freeze, R.A.; Cherry, J.A. *Groundwater*; Prentice-Hall: Englewood Cliffs, NJ, USA, 1979.
38. Terrenghi, J. Flusso Idrico E Trasporto Reattivo Di Contaminanti In Acquiferi Eterogenei E Applicazioni. PhD Thesis, Università degli Studi di Milano, Milan, Italy, 2018. (In Italian). [CrossRef]
39. ISS-INAIL ISS-INAIL Database for Environmental Health Risk Analysis. Online Database. Available online: https://www.isprambiente.gov.it/it/attivita/suolo-e-territorio/siti-contaminati/analisi-di-rischio (accessed on 1 May 2022). (In Italian)
40. Christensen, T.H.; Bjerg, P.L.; Banwart, S.A.; Jakobsen, R.; Heron, G.; Albrechtsen, H.-J. Characterization of Redox Conditions in Groundwater Contaminant Plumes. *J. Contam. Hydrol.* **2000**, *45*, 165–241. [CrossRef]
41. Hyun, S.P.; Hayes, K.F. Feasibility of Using In Situ FeS Precipitation for TCE Degradation. *J. Environ. Eng.* **2009**, *135*, 1009–1014. [CrossRef]
42. D'Affonseca, F.M.; Prommer, H.; Finkel, M.; Blum, P.; Grathwohl, P. Modeling the Long-Term and Transient Evolution of Biogeochemical and Isotopic Signatures in Coal Tar-Contaminated Aquifers: Modeling Coal Tar-Contaminated Aquifers. *Water Resour. Res.* **2011**, *47*, 22. [CrossRef]
43. He, Y.T.; Wilson, J.T.; Su, C.; Wilkin, R.T. Review of Abiotic Degradation of Chlorinated Solvents by Reactive Iron Minerals in Aquifers. *Groundw. Monit. Remediat.* **2015**, *35*, 57–75. [CrossRef]
44. Dalla Libera, N.; Fabbri, P.; Mason, L.; Piccinini, L.; Pola, M. A Local Natural Background Level Concept to Improve the Natural Background Level: A Case Study on the Drainage Basin of the Venetian Lagoon in Northeastern Italy. *Environ. Earth Sci.* **2018**, *77*, 487. [CrossRef]
45. Slater, G.F.; Sherwood Lollar, B.; Sleep, B.E.; Edwards, E.A. Variability in Carbon Isotopic Fractionation during Biodegradation of Chlorinated Ethenes: Implications for Field Applications. *Environ. Sci. Technol.* **2001**, *35*, 901–907. [CrossRef]
46. Cichocka, D.; Siegert, M.; Imfeld, G.; Andert, J.; Beck, K.; Diekert, G.; Richnow, H.-H.; Nijenhuis, I. Factors Controlling the Carbon Isotope Fractionation of Tetra- and Trichloroethene during Reductive Dechlorination by Sulfurospirillum Ssp. and Desulfitobacterium Sp. Strain PCE-S: Carbon Isotope Fractionation during Reductive Dechlorination. *FEMS Microbiol. Ecol.* **2007**, *62*, 98–107. [CrossRef]
47. Liang, X.; Dong, Y.; Kuder, T.; Krumholz, L.R.; Philp, R.P.; Butler, E.C. Distinguishing Abiotic and Biotic Transformation of Tetrachloroethylene and Trichloroethylene by Stable Carbon Isotope Fractionation. *Environ. Sci. Technol.* **2007**, *41*, 7094–7100. [CrossRef]
48. Wiegert, C.; Mandalakis, M.; Knowles, T.; Polymenakou, P.N.; Aeppli, C.; Macháčková, J.; Holmstrand, H.; Evershed, R.P.; Pancost, R.D.; Gustafsson, Ö. Carbon and Chlorine Isotope Fractionation During Microbial Degradation of Tetra- and Trichloroethene. *Environ. Sci. Technol.* **2013**, *47*, 6449–6456. [CrossRef]
49. Renpenning, J.; Hitzfeld, K.L.; Gilevska, T.; Nijenhuis, I.; Gehre, M.; Richnow, H.-H. Development and Validation of an Universal Interface for Compound-Specific Stable Isotope Analysis of Chlorine (^{37} Cl/ ^{35} Cl) by GC-High-Temperature Conversion (HTC)-MS/IRMS. *Anal. Chem.* **2015**, *87*, 2832–2839. [CrossRef]
50. Hourbron, E.; Escoffier, S.; Capdeville, B. Trichloroethylene Elimination Assay by Naural Consortia of Heterotrophic and Methanotrophic Bacteria. *Water Sci. Technol.* **2000**, *42*, 395–402. [CrossRef]
51. Powell, C.L.; Goltz, M.N.; Agrawal, A. Degradation Kinetics of Chlorinated Aliphatic Hydrocarbons by Methane Oxidizers Naturally-Associated with Wetland Plant Roots. *J. Contam. Hydrol.* **2014**, *170*, 68–75. [CrossRef]
52. Zalesak, M.; Ruzicka, J.; Vicha, R.; Dvorackova, M. Cometabolic Degradation of Dichloroethenes by Comamonas Testosteroni RF2. *Chemosphere* **2017**, *186*, 919–927. [CrossRef] [PubMed]
53. Wang, C.-C.; Li, C.-H.; Yang, C.-F. Acclimated Methanotrophic Consortia for Aerobic Co-Metabolism of Trichloroethene with Methane. *Int. Biodeterior. Biodegrad.* **2019**, *142*, 52–57. [CrossRef]

54. Ryoo, D.; Shim, H.; Canada, K.; Barbieri, P.; Wood, T.K. Aerobic Degradation of Tetrachloroethylene by Toluene-o-Xylene Monooxygenase of Pseudomonas Stutzeri OX1. *Nat. Biotechnol.* **2000**, *18*, 775–778. [CrossRef]
55. Zimmermann, J.; Halloran, L.J.S.; Hunkeler, D. Tracking Chlorinated Contaminants in the Subsurface Using Compound-Specific Chlorine Isotope Analysis: A Review of Principles, Current Challenges and Applications. *Chemosphere* **2020**, *244*, 125476. [CrossRef] [PubMed]
56. Huang, L.; Sturchio, N.C.; Abrajano, T.; Heraty, L.J.; Holt, B.D. Carbon and Chlorine Isotope Fractionation of Chlorinated Aliphatic Hydrocarbons by Evaporation. *Org. Geochem.* **1999**, *30*, 777–785. [CrossRef]
57. Poulson, S.R.; Drever, J.I. Stable Isotope (C, Cl, and H) Fractionation during Vaporization of Trichloroethylene. *Environ. Sci. Technol.* **1999**, *33*, 3689–3694. [CrossRef]
58. Jeannottat, S.; Hunkeler, D. Chlorine and Carbon Isotopes Fractionation during Volatilization and Diffusive Transport of Trichloroethene in the Unsaturated Zone. *Environ. Sci. Technol.* **2012**, *46*, 3169–3176. [CrossRef]
59. Chapelle, F.H.; Haack, S.K.; Adriaens, P.; Henry, M.A.; Bradley, P.M. Comparison of E_h and H_2 Measurements for Delineating Redox Processes in a Contaminated Aquifer. *Environ. Sci. Technol.* **1996**, *30*, 3565–3569. [CrossRef]
60. Kouznetsova, I.; Mao, X.; Robinson, C.; Barry, D.A.; Gerhard, J.I.; McCarty, P.L. Biological Reduction of Chlorinated Solvents: Batch-Scale Geochemical Modeling. *Adv. Water Resour.* **2010**, *33*, 969–986. [CrossRef]
61. Maillard, J.; Schumacher, W.; Vazquez, F.; Regeard, C.; Hagen, W.R.; Holliger, C. Characterization of the Corrinoid Iron-Sulfur ProteinTetrachloroethene Reductive Dehalogenase of *Dehalobacterrestrictus*. *Appl. Environ. Microbiol.* **2003**, *69*, 4628–4638. [CrossRef]
62. Yu, S.; Semprini, L. Kinetics and Modeling of Reductive Dechlorination at High PCE and TCE Concentrations. *Biotechnol. Bioeng.* **2004**, *88*, 451–464. [CrossRef] [PubMed]
63. Amos, B.K.; Christ, J.A.; Abriola, L.M.; Pennell, K.D.; Löffler, F.E. Experimental Evaluation and Mathematical Modeling of Microbially Enhanced Tetrachloroethene (PCE) Dissolution. *Environ. Sci. Technol.* **2007**, *41*, 963–970. [CrossRef] [PubMed]
64. Cupples, A.M.; Spormann, A.M.; McCarty, P.L. Comparative Evaluation of Chloroethene Dechlorination to Ethene by *Dehalococcoides* -like Microorganisms. *Environ. Sci. Technol.* **2004**, *38*, 4768–4774. [CrossRef]
65. Widdowson, M.A. Modeling Natural Attenuation of Chlorinated Ethenes Under Spatially Varying Redox Conditions. *Biodegradation* **2004**, *15*, 435–451. [CrossRef]
66. Yu, S.; Dolan, M.E.; Semprini, L. Kinetics and Inhibition of Reductive Dechlorination of Chlorinated Ethylenes by Two Different Mixed Cultures. *Environ. Sci. Technol.* **2005**, *39*, 195–205. [CrossRef] [PubMed]
67. van Warmerdam, E.M.; Frape, S.K.; Aravena, R.; Drimmie, R.J.; Flatt, H.; Cherry, J.A. Stable Chlorine and Carbon Isotope Measurements of Selected Chlorinated Organic Solvents. *Appl. Geochem.* **1995**, *10*, 547–552. [CrossRef]
68. Abe, Y.; Aravena, R.; Zopfi, J.; Shouakar-Stash, O.; Cox, E.; Roberts, J.D.; Hunkeler, D. Carbon and Chlorine Isotope Fractionation during Aerobic Oxidation and Reductive Dechlorination of Vinyl Chloride and Cis-1,2-Dichloroethene. *Environ. Sci. Technol.* **2009**, *43*, 101–107. [CrossRef]
69. Kuder, T.; Philp, P.; Van Breukelen, B.; Thouement, H.A.A.; Vanderford, M.; Newell, C.J. Integrated Stable Isotope—Reactive Transport Model Approach for Assessment of Chlorinated Solvent Degradation. *Technical Report*, 2014.